Parametric amplification of short pulses in optical fiber Bragg gratings

M. J. Steel and C. Martijn de Sterke
School of Physics, University of Sydney, New South Wales 2006, Australia
and Australian Photonics Cooperative Research Centre, 101 National Innovation Centre, Australian Technology Park, Eveleigh, New South Wales 1430, Australia
(Received 18 April 1996)

We study $\chi^{(3)}$ parametric amplification of a weak signal pulse tuned to a Bragg grating through a series of numerical simulations. These simulations demonstrate that gratings permit strong signal amplification for large wave vector mismatches between pump, signal, and idler, even though gain would be prohibited in the corresponding uniform medium. The enhanced gain is explained in terms of a shift in the signal wave vector due to the strong dispersion induced by the grating, an effect which is well known from other frequency conversion processes. For $\chi^{(3)}$ parametric amplification, the pulsed regime introduces several new effects, many of which are explained by simple arguments based on the cw dispersion relation of the grating. Notably, the gain exhibits a ''self-locking'' behavior, in that there is considerable freedom in the input frequency of the signal. [S1063-651X(96)06909-7]

PACS number(s): 42.65.Ky, 42.65.Hw

I. INTRODUCTION

The study of short optical pulses in Bragg gratings has been dominated by two broad areas. In the linear regime, one of the main themes has been that of dispersion compensation in chirped optical fiber Bragg gratings for long-haul communications. Proposed some time ago [1], this has now been clearly demonstrated [2–4]. In the nonlinear regime, theoretical studies of switching [5] and gap solitons occupy most of a now considerable literature (see Ref. [6] for a recent review). Behind this nonlinear work is the fundamental idea that light tuned close to the Bragg resonance, which would be reflected at low intensities, may at sufficiently high intensities tune itself out of the band gap and thus be transmitted, exhibiting solitonlike propagation. Both bistability [7–9], and gap solitons or ''Bragg grating solitons'' [10] have now been observed experimentally.

An area of nonlinear processes in Bragg gratings that has received much less attention is the interaction between a strong pump pulse and a weak signal pulse inside a grating. Several authors have considered pump-induced switching of a cw signal by a pump detuned from the grating [11,12] and the concept has received a first demonstration [13]. In other work, we treated the case where the pump and signal are both pulses and are widely separated in frequency [14,15]. Whereas the signal is tuned to the grating and travels with a group velocity much less than the speed of light, the pump propagates unimpeded at the speed of light in the medium. Under these conditions, it was found that although if both the pump and signal are weak, the pump overtakes and passes through the signal; a high intensity pump produces substantial reshaping of the signal. Through cross-phase modulation (XPM), the signal is shifted to lower frequencies on the grating dispersion relation where the group velocity is larger, and in addition the signal becomes chirped. Thus the average frequency shift causes the signal to accelerate and keep up with the pump, while the chirp and grating dispersion lead to compression of the signal. The net effect is to see the compressed signal swept out of the grating on the leading edge of the pump—the so-called ''optical pushbroom.'' The frequency separation is required to be large to guarantee that the only nonlinear interaction is XPM.

Recently, we have studied a more complex problem in which the geometry is unchanged but we relax the condition of large frequency separation between the pump and signal [16]. This allows the nonlinear process of four wave mixing or parametric amplification to occur according to the relation $\omega_p+\omega_p=\omega_s+\omega_i$, in which two pump photons of frequency ω_p are converted to one photon each at the signal ω_s and idler ω_i frequencies. The frequencies are separated by the quantity

$$\Delta\omega=\omega_s-\omega_p=\omega_p-\omega_i. \tag{1}$$

Note that although the fields are now more closely spaced in frequency, we still assume that only the signal frequency is affected by the grating (see Fig. 1). We demonstrate below

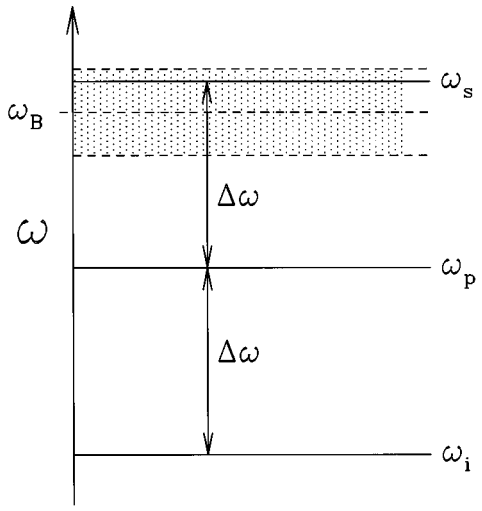

FIG. 1. Schematic of the frequencies involved in the parametric amplification system.

that such a situation indeed occurs in optical fibers. The relative efficiency of the process is governed by the wave vector mismatch parameter

$$\Delta = k_s + k_i - 2k_p, \tag{2}$$

where k_s, k_i, k_p are the wave vectors corresponding to the frequencies $\omega_s, \omega_i, \omega_p$. In the absence of the grating, amplification of the signal only occurs for a limited range of the mismatch Δ, dependent on the pump power [17]. Although the detailed dynamics when the grating is included are highly involved, in our previous work we found very general behavior for a wide range of parameters [16]. In short, the inclusion of the grating allows amplification of the signal and idler by the pump for a large range of parameters that would not permit growth without the grating. Providing Δ is not too large, the purely compressive effect seen in the optical pushbroom [14,15] is swamped by amplification of the signal. Moreover, in contrast to the optical pushbroom where the signal sits on the leading edge of the pump pulse, when parametric amplification is able to operate, the signal becomes located on the trailing edge of the pump.

The enhancement in gain is a result of ''grating-assisted phase matching,'' an effect which is well known for frequency conversion processes in the continuous wave (cw) regime [18–25]. Adding a grating introduces strong dispersion near the Bragg resonance so that the wave vector of any field tuned to the grating varies much more rapidly with frequency than in the uniform medium. The mismatch Δ thus changes and so the grating influences the efficiency of the frequency conversion. In fact, for particular detunings from the resonance, efficient conversion may become possible between frequencies that would not be phase matched in the uniform medium. Many frequency conversion processes are governed by phase matching conditions and hence a grating may enhance any of these processes. Several authors have studied the influence of a grating on cw second harmonic generation (SHG) through a $\chi^{(2)}$ nonlinearity [20–25]. In general, one finds enhancement of the harmonic for frequencies on one side of the Bragg resonance where the grating achieves phase matching. On the other side of the Bragg resonance, the grating worsens the phase matching and there is minimal output [21,25]. These predictions have been verified experimentally for SHG in semiconductor gratings [26]. A similar enhancement in gain is predicted to occur for cw parametric amplification with a $\chi^{(3)}$ nonlinearity [19], though with several complications over the SHG problem: through XPM the signal experiences a nonlinear change in the refractive index which causes the enhancement of the gain to be shifted to lower frequencies (assuming a positive nonlinearity). Moreover, unlike the SHG case, the degree of enhancement depends on the input pump power. Finally, in the absence of the grating [17], parametric gain occurs over a range of values of Δ, whereas in SHG, the relevant mismatch parameter is required to vanish identically to achieve phase matching. This difference is mirrored when a grating is included.

Whereas the continuous wave regime of frequency conversion in gratings has attracted much attention, as far as we are aware our previous paper (see Ref. [15]) is the only study that has considered short pulses. In the undepleted pump approximation, the cw problem for SHG is described by a driven linear system. Hence, pulsed SHG in gratings can be reduced to a Fourier superposition of the cw response and we would not expect qualitatively new results. In contrast, as our earlier work showed [16], new effects are found with pulsed $\chi^{(3)}$ parametric amplification. Notably, the gain becomes ''self-locking''—the input signal need not be tuned to the frequency at which the grating produces phase matching. Rather, cross-phase modulation ensures that this frequency is generated automatically.

Including general time dependence into the problem of parametric amplification in Bragg gratings leads to a system that is resistant to analytic techniques; note for instance that we have no natural nonlinear modes on which to build a perturbation theory as has been done for problems of perturbed gap solitons [27]. In our previous work therefore [16], we studied the system through numerical simulations. We continue this approach in this paper, but in much greater detail. We begin by showing further examples of the enhancement of the signal gain to illustrate the wide variety of parameters for which it occurs. We then demonstrate that the enhancement is indeed a result of grating-assisted phase matching. We also explore and explain trends in several aspects of the gain as the system parameters are varied. These aspects include the time taken for the gain to begin, the rate of gain, and the width of the signal and idler pulses during the amplification. Although the parameter space for the problem is very large, we nevertheless provide physical explanations for virtually all the qualitative features we observe. Thus although fully quantitative results must be found from complete simulations, a sound physical knowledge of this system is still attainable.

The remainder of the paper is structured as follows. In Sec. II we present the relevant features of previous work on cw frequency conversion in gratings. Our fully time-dependent model is presented in Sec. III where we recall the behavior of pulses undergoing parametric amplification in uniform media, while in Sec. IV we map out the parameter space to be explored when the grating is included. Sec. V contains the results of our simulations and demonstrations of the action of the grating in achieving phase matching. In Sec. VI we discuss a number of trends in physical properties observed in the simulations. Finally in Sec. VII we briefly discuss some additional points.

II. PROPERTIES OF BRAGG-ASSISTED CONTINUOUS WAVE FREQUENCY CONVERSION

We now summarize the properties of cw parametric amplification in gratings [19], which remain relevant in the pulsed case. We begin, however, with the simpler case of parametric amplification in a uniform medium.

A. Grating-free parametric amplification

The mismatch parameter Δ is a linear property of the medium that depends on the intrinsic material (and waveguide) dispersion of the medium. On the other hand, the phase-matching condition required for gain depends on the details of the nonlinear interaction. For parametric amplification with a $\chi^{(3)}$ nonlinearity in the absence of the grating [17], the signal experiences gain if

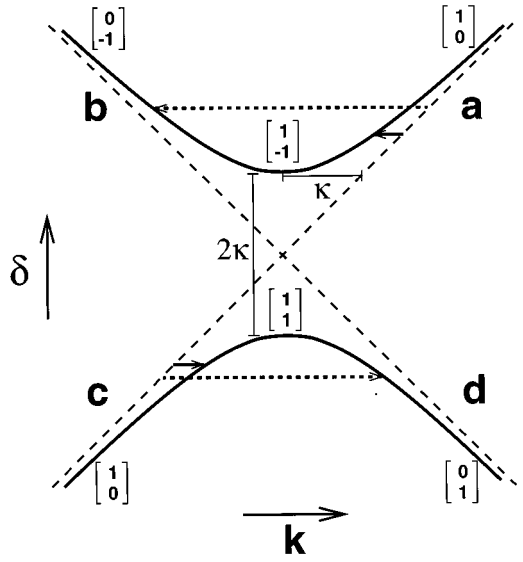

FIG. 2. Dispersion relation for a Bragg grating (solid) superposed on uniform medium dispersion relation (dotted). Column vectors indicate the Bloch vectors $\mathbf{f}=(f_+,f_-)$ describing the relative strength of forward (f_+) and backward (f_-) plane waves in the Bloch functions at different points on the dispersion relation. Solid horizontal lines indicate wave vector shifts to the near branches (labeled a and c), of the dispersion relation. Dotted horizontal lines indicate shifts to the far branches (labeled b and d).

$$-4\tilde{\mu}\leqslant\Delta\leqslant 0, \tag{3}$$

where we have defined the nonlinear detuning

$$\tilde{\mu}=\Gamma|P|^2, \tag{4}$$

in terms of the pump amplitude P and the nonlinear coefficient $\Gamma=3\omega_s\chi^{(3)}/(2cn)$, where c is the speed of light *in vacuo* and n is the refractive index of the medium. The amplification is most efficient when

$$\Delta=-2\tilde{\mu}. \tag{5}$$

This equation represents an exact balance between the wave vector mismatch that results from the material dispersion, and an additional nonlinear wave vector mismatch induced by cross-phase modulation [17].

B. Effects with a grating

Most of the effects of the grating on phase matching can be understood from Fig. 2 which shows the dispersion relation of a uniform Bragg grating (solid line) superposed on the straight line dispersion relation of the corresponding uniform medium (dashed line). The vertical axis is represented in terms of the detuning from the Bragg resonance

$$\delta=\frac{\omega-\omega_{\mathrm{B}}}{v_g}. \tag{6}$$

Here v_g is the group velocity of the signal in the uniform medium, and $\omega_{\mathrm{B}}=\pi c/(\overline{n}d)$ is the resonant Bragg frequency, with d and $\overline{n}$ the period and average index of the grating, respectively. The uniform medium dispersion relation of course does not have constant slope over all frequencies—it curves due to the dispersion which gives rise to the wave vector mismatch in the first place. Over the bandwidth of the grating, however, the intrinsic dispersion is negligible. This is especially true in optical fibers for which the grating depth is modest and the bandwidth affected by the grating relatively narrow—the deepest made so far have a relative bandwidth of $\Delta\lambda/\lambda\lesssim 0.01$. The properties of the grating dispersion relation are well known—the periodicity opens up a photonic band gap representing frequencies for which traveling waves are forbidden and light is reflected. The gap has width $2v_g\kappa$ where the coupling strength $\kappa=\omega\Delta n/(2c)$ with Δn the refractive index modulation of the grating. Outside the gap, traveling waves are allowed, but the dispersion relation is strongly curved with the group velocity given by its slope (see Fig. 2).

For our purposes, the most important consequence of the grating is indicated by the horizontal arrows in Fig. 2. When compared to its wave vector in the uniform medium, light of a particular frequency experiences a shift in wave vector of size [18–22]

$$\Delta k_s=-\delta\pm\sqrt{\delta^2-\kappa^2}. \tag{7}$$

The choice of sign reflects the fact that the grating allows light to exist on either of two branches for any detuning, with the upper sign taken for the branches to the right of the Bragg wave number $k_{\mathrm{B}}=\omega_{\mathrm{B}}\overline{n}/c$. Note from Fig. 2 that the shift is negative for frequencies above the band gap ($\delta>\kappa$), and positive for frequencies below the gap ($\delta<-\kappa$). Further the shift may be greater or smaller than the coupling strength κ: Shifts of $|\Delta k_s|<\kappa$ are achieved on the branch near the uniform medium line (indicated by the solid arrows and the labels a and c in Fig. 2); shifts of $|\Delta k_s|>\kappa$ are achieved on the far branch (indicated by the dotted arrows and the labels b and d in Fig. 2), and simply by taking $|\delta|$ large enough, a wave vector shift of arbitrary size and sign is obtained regardless of the grating strength! Thus although the phase matching condition may not be satisfied in the uniform medium, in the grating there is a change to the mismatch parameter due to the shift in the signal wave vector so that phase matching may be possible permitting efficient conversion [21]. From Eq. (7) we find that for any given Δk_s, the signal is phase matched at the unique detuning

$$\delta=-\frac{(\Delta k_s)^2+\kappa^2}{2\Delta k_s}. \tag{8}$$

In principle then, at the correct detuning the grating produces phase matching for any initial mismatch Δ.

This result is at first sight surprising—we would not expect that a weak grating should significantly enhance the gain at a frequency far detuned from the Bragg resonance. The resolution lies in noting that phase matching is not of itself sufficient to produce gain—there must be a reasonable longitudinal mode overlap between the pump and signal modes. While the modes of a uniform medium are forward- and backward-traveling plane waves, the modes inside a

grating are Bloch functions [28]. For shallow gratings, the Bloch functions ψ are superpositions of plane waves of the form

$$\psi = f_+ \exp(ik_s z) + f_- \exp(-ik_s z), \tag{9}$$

where the amplitudes $f_\pm$ are functions of frequency but not of position. Thus we can represent any Bloch function in terms of the amplitudes f_+ and f_- of the forward and backward plane waves by the unit column vector $\mathbf{f}=(f_+,f_-)$. The (unnormalized) Bloch functions for various points are indicated by the column vectors in Fig. 2. Far from the grating the Bloch functions are approximately plane waves, while at the band edges they are standing waves. Now typically the pump, which is detuned from the grating (see Fig. 1), propagates as a forward plane wave, whereas the signal occupies a Bloch function determined by its detuning δ. If the wave vector shift needed to achieve phase matching is small relative to κ, the signal is in a Bloch function which is relatively close to a forward plane wave (branches a or c) and there is large gain. For a very large wave vector shift to the distant branches (b or d), the relevant Bloch function is virtually a backward plane wave. The pump and signal are then almost orthogonal and there is negligible gain. For intermediate shifts at points near the band edge, the Bloch functions on both branches are an equal combination of forward and backward plane waves and there is an intermediate degree of gain [18,19,21,25]. These results can be represented geometrically if the Bloch vector **f** is considered as a vector in a real two-dimensional space. As a forward plane wave, the pump mode is represented by the vector (1,0). The signal is represented by the vector **f** corresponding to its position on the dispersion relation. Then given Δk_s, if the signal is detuned for perfect phase matching according to Eq. (8), the angle α between the pump vector and **f** is given by

$$\tan\alpha = \left| \frac{\Delta k_s}{\kappa} \right|. \tag{10}$$

So for $|\Delta k_s| \ll \kappa$, α is small and the two vectors are almost parallel giving large coupling. For $|\Delta k_s| \gg \kappa$, $\alpha \lesssim \pi/2$ so the vectors are almost orthogonal and there is negligible coupling. All the effects in this section play roles in the pulsed results for parametric amplification as shown in Sec. V.

Note that the description here has made no mention of the pump power. This is accurate for cw second harmonic generation in gratings—increasing the pump power increases the second harmonic intensity in proportion but does not affect the phase-matching arguments [21,24,25]. For cw parametric amplification, however, this is an oversimplification. A full treatment [19] shows that the detuning for maximum signal amplification depends on the pump power [see Eq. (4)], and thus Eq. (8) does not give exactly the detuning for maximum gain. This effect is not of importance for our purposes here and the basic manner in which the grating produces wave vector shifts remains valid.

III. MATHEMATICAL MODEL

We now present the coupled mode equations that comprise our model. Recalling that we assume that only the signal field is tuned to the grating, we write the electric field as

$$E = [E_+ \exp(ik_s z) + E_- \exp(-ik_s z)] \exp(-i\omega_s t) + P \exp[i(k_p z - \omega_p t)] + I \exp[i(k_i z - \omega_i t)] + \text{c.c.}, \tag{11}$$

where E_+, E_-, P, I are the slowly varying amplitudes of the forward- and backward-moving signal fields, and forward-moving pump and idler fields (see Fig. 1). We neglect backward-moving fields for the pump and idler which experience negligible reflection from the grating, and write the refractive index as

$$n(\omega) = \overline{n(\omega)} + \Delta n \cos\left(\frac{2\pi z}{d}\right), \tag{12}$$

with $\overline{n(\omega)}$ the mean index of the grating. Substituting Eqs. (11) and (12) in the wave equation, we make the undepleted pump approximation and other standard approximations to reach the system [19]

$$+ i\frac{\partial E_+}{\partial z} + \frac{i}{v_g}\frac{\partial E_+}{\partial t} + \frac{1}{2}\frac{\omega''}{v_g}\frac{\partial^2 E_+}{\partial z^2} + \kappa E_- + \Gamma[2|P|^2 E_+ + \exp(-i\Delta z) P^2 I^*] = 0, \tag{13a}$$

$$-i\frac{\partial E_-}{\partial z} + \frac{i}{v_g}\frac{\partial E_-}{\partial t} + \frac{1}{2}\frac{\omega''}{v_g}\frac{\partial^2 E_-}{\partial z^2} + \kappa E_+ + 2\Gamma|P|^2 E_- = 0, \tag{13b}$$

$$+ i\frac{\partial I}{\partial z} + \frac{i}{v_i}\frac{\partial I}{\partial t} + \frac{1}{2}\frac{\omega_i''}{v_i}\frac{\partial^2 I}{\partial z^2} + \Gamma_i[2|P|^2 I + \exp(-i\Delta z) P^2 E_+^*] = 0, \tag{13c}$$

$$+ i\frac{\partial P}{\partial z} + \frac{i}{v_p}\frac{\partial P}{\partial t} + \frac{1}{2}\frac{\omega_p''}{v_p}\frac{\partial^2 P}{\partial z^2} + \Gamma_p|P|^2 P = 0. \tag{13d}$$

Here v_g, v_i and v_p, and Γ, Γ_i, and Γ_p are the group velocities and nonlinear coefficients at the signal frequency, idler and pump frequencies, respectively. From hereon, we adopt the approximation that these quantities are the same for all three frequencies and drop the subscripts. In particular, we can assume the group velocities are the same as the degree of walk off over the length of a grating is negligible [17]. It is then convenient to rescale the time variable introducing the quantity $T = v_g t$. The symbols ω'', ω_p'', and ω_i'' represent the intrinsic material dispersion at the three frequencies. Finally, the nonlinearity is taken to be positive.

Note that due to the undepleted pump assumption, Eq. (13d) is uncoupled from the other three. Also, E_- experiences gain only indirectly through the grating coupling to E_+. We can make an additional simplification by noting that for a typical grating geometry the second derivative terms representing intrinsic dispersion are negligible. This is discussed in detail below.

It is useful for understanding later results to examine briefly the response of the system in the absence of the grating. In this case the second derivative terms in Eqs. (13) are the dominant source of dispersion, and we are not strictly justified in omitting them. For distances comparable to typical grating lengths of a few centimeters, however, it is again

an excellent approximation. Without the grating, E_- plays no role in the gain process and Eq. (13b) may be dropped. By a trivial transformation, the remaining three equations reduce to the well known time-independent case [17] and the general solution may be written down directly. While the precise form of the solution is not important here, we note that the pump propagates with a constant profile such that

$$|P(z,T)|=f(\zeta), \tag{14}$$

where $\zeta=z-T$ is a position coordinate in the frame moving with the pump. By analogy with Eq. (4), it is helpful to introduce a position-dependent detuning

$$\mu(\zeta)=\Gamma f^2(\zeta). \tag{15}$$

Further, without loss of generality, we may take the pump profile $f(\zeta)$ to have its peak at $\zeta=0$ and define the maximum nonlinear detuning by

$$\mu_{\max}\equiv\mu(0)=\Gamma f^2(0). \tag{16}$$

The gain experienced by the signal due to the pump is given by

$$g(\zeta)=v\sqrt{-\Delta\Gamma f^2(\zeta)-\Delta^2/4}. \tag{17}$$

The signal is amplified for all ζ (if any), where g is real. If g is real and T is large, the signal grows approximately as $|E(\zeta,T)|\approx\exp[g(\zeta)T]$. For each point ζ on the pump, this occurs for the range of wave vector mismatch

$$-4\mu(\zeta)<\Delta<0, \tag{18}$$

with the maximum gain at

$$\Delta=-2\mu(\zeta), \tag{19}$$

[cf. Eqs. (3) and (5)]. Note however, from Eq. (17) that for a particular value of Δ, the gain increases monotonically with pump power. Thus provided the peak detuning $\mu_{\max}$ is sufficient to produce gain at all [i.e., $f^2(\zeta)>-\Delta/(4\Gamma)$], the gain is strongest at the peak of the pump. This has the consequence that regardless of the initial relative positions of the pump and signal, the signal width decreases with time and its peak becomes coincident with that of the pump. This contrasts with the optical pushbroom described in Sec. I in which the signal sits on the leading edge of the pump. For Δ outside the range in Eq. (18), g is imaginary and the pulses develop rapid oscillations but do not grow in amplitude.

IV. PARAMETER SPACE

We now set out the parameters to be explored in the next section. Although we cannot span the entire parameter space which includes pulse widths, grating strengths, pump powers, and wave vector mismatch, we point out that the qualitative behavior of the system is robust to quite large variations in parameters and thus the physical arguments behind the simulations we describe are quite general. Throughout we use dimensionless units, but shortly we do make the connection to a typical optical fiber geometry to demonstrate that our choice of parameters is realistic. As Eq. (13d) remains uncoupled from the other coupled mode equations (13), the pump field remains unchanged from the grating-free case. We take the initial pump and signal pulses to have Gaussian profiles, with a pump width of $w_p=2$ and initial signal width of $w_s=3$. The nonlinear detuning has a peak strength $\mu_{\max}=2$. The pump and signal are initially coincident and the initial idler field is zero. Propagation occurs for a time $T=15$. These parameters are the same for all calculations. From Sec. III, in the absence of the grating we would expect gain in the range $-8=-4\mu_{\max}<\Delta<0$ with maximum gain for $\Delta=-4$ [see Eqs. (18) and (19)]. We perform simulations for a range centered around this value such that $-16\leqslant\Delta\leqslant 8$. As we can expect interesting results when the coupling strength is comparable to the wave vector mismatch, for each value of Δ we perform one simulation for each integer value of κ in the range 0–16. The simulations thus lie in a two dimensional $\Delta-\kappa$ plane. Anticipating our results, it is helpful to introduce one further parameter

$$\epsilon=-2\mu_{\max}-\Delta, \tag{20}$$

which is a measure of how well the system would be phase matched in the absence of the grating—perfect phase matching corresponds to $\epsilon=0$ [cf. Eq. (19)]. For the peak pump strength $\mu_{\max}=2$ in our system, the weak fields experience gain in the nongrating case if $|\epsilon|\leqslant 4$, while the behavior is oscillatory for $|\epsilon|>4$.

As an example of a real system described by our model we consider optical fiber gratings. Taking the unit of length as the centimeter, we find that the time unit is 50 ps, so that the pump and initial signal widths are 100 ps and 150 ps, respectively. A propagation time of 750 ps would require a grating of length $L=15-20$ cm. Gratings at the lower end of this range are available now. For a mode area of $A_{\text{eff}}=20\ \mu\text{m}^2$, the peak pump power $\mu_{\max}=2$ is equivalent to an actual power of 30 kW or an intensity of 150 GWm^{-2}. A mode-locked Nd:YAG laser at 1.064 μm would thus be a suitable pump source. In fact, a similar Nd:YLF laser with powers in this range was used in recent experiments to observe grating solitons [10]. The wave vector mismatch takes the range $-16\ \text{cm}^{-1}\leqslant\Delta\leqslant 8\ \text{cm}^{-1}$. The dependence of Δ on the frequency separation $\Delta\omega$ for a typical optical fiber is illustrated in Fig. 3. Each curve gives Δ as a function of pump wavelength λ_p for a given frequency separation $\Delta\omega$ which is marked as a fraction of $10^{15}\ \text{s}^{-1}$. The curves were calculated by solving the eigenvalue equation for the fiber modes [17,29]. Two significant wavelengths are indicated. It is also clear that Δ changes sign at the zero dispersion wavelength near 1.27 μm. The figure indicates that the range of Δ in our simulations corresponds to frequency separations of the order $\Delta\omega=0.05\times10^{15}\ \text{s}^{-1}$ to $0.25\times10^{15}\ \text{s}^{-1}$. The case $\Delta=0$ is somewhat problematic as from Fig. 3, we find this can only occur for $\Delta\omega=0$ which is not consistent with a frequency conversion process! In a medium with a more complicated dispersion relation, however, it is conceivable that $\Delta=0$ could be achieved for some nonzero frequency separation and hence we retain this value. The grating depth κ also takes realistic values: it ranges from $\kappa=0$ (the ''empty'' grating), to $\kappa=16\ \text{cm}^{-1}$, corresponding to a relatively modest index modulation of $\Delta n=5\times10^{-4}$.

We can also demonstrate the validity of the approximations we have made. The pump and idler are assumed to be

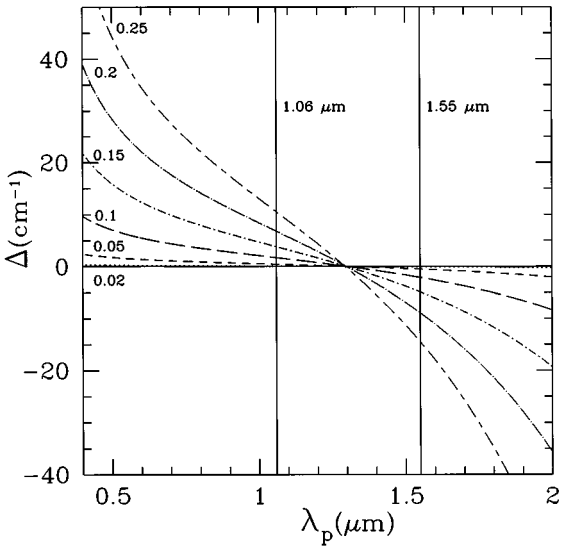

FIG. 3. Wave vector mismatch Δ as a function of λ_p. Each curve is marked with a frequency separation $\Delta\omega$ measured in 10^{15} s^{-1}.

unaffected by the grating in Eqs. (13). Even for the smallest frequency separation and strongest grating described above, the pump is detuned from the grating by greater than 150 $v_g\kappa$. For such a separation, both the reflective and dispersive properties of the grating are negligible and our assumption is justified. It is simple to check that spectral broadening of the pump due to self-phase modulation (SPM) does not significantly affect this conclusion over the short propagation lengths considered [17]. In addition, in our simulations we neglect the effects of material dispersion described by the second derivatives in Eqs. (13). This is easily justified by consideration of the relative scale lengths over which SPM and dispersion can play a significant role. The characteristic nonlinear length [17] $L_{NL}=1/(\Gamma P^2)=0.5$ cm is of the same order as the pulse length. In contrast, for a typical value of the group velocity dispersion of $|\beta_2|\equiv|d^2k/d\omega^2|\approx 20$ ps^2/km at 1.064 μm or 1.55 μm with the pulse width $w_p \approx 100$ ps, the dispersion length [17] $L_D\equiv w_p^2/|\beta_2|\approx 500$ km$\gg L_{\mathrm{NL}}, L$, and so the dispersive terms can be safely neglected for propagation lengths of a few centimeters. Note of course, that the material dispersion gives rise to the mismatch parameter Δ. Thus while we neglect dispersion over the bandwidth of a particular pulse, we do not neglect its effects over the much larger frequency separation of the different fields.

The simulations were performed using an extension of a collocation method described in Ref. [30]. This is made possible by dropping the second derivative terms in Eqs. (13) so that the characteristics are straight lines, permitting a considerable speed improvement over split-step methods.

V. RESULTS

A. Evolution of fields

We begin our results with a time sequence of the evolving fields for a typical case. We choose parameters such that the signal would lie outside the gain band in the absence of the grating. Figures 4(a)–4(f) show the fields as a function of position at six different times for the parameters $\Delta=-16$, $\kappa=8$. For this case $\epsilon=12$ [see Eq. (20)], so that the signal is well outside the gain band. In this figure and later illustrations of fields, the line styles indicate the fields as follows: E_+—solid line, E_-—dot-dashed, P—dotted, and I—dashed. Note that the horizontal axes shift as time progresses and that the vertical scales refer to the moduli of the signal and idler amplitudes. The pump is of course much more intense than the other low-power fields and is shown at a different scale. The initial configuration appears in Fig. 4(a) with the pump and forward signal E_+ coincident, and the backward signal E_- and idler set to zero. Figs. 4(b)–4(d) show the fields at $T=2.5$, $T=5$, and $T=10$, respectively. The idler begins to be generated by interaction of E_+ and P while the grating couples energy between the forward and backward signal. The bulk of the energy in the signal and idler gradually becomes concentrated on the rear of the pump. In this period the field structures are complicated and change rapidly with time, and only modest growth occurs. By $T=12.5$ [Fig. 4(e)], substantial growth has occurred and all three weak fields are localized on the rear of the pump and have a regular single peaked shape. As propagation continues to $T=15$ [Fig. 4(f)], the signal and idler fields experience further growth but the field profiles remain virtually unchanged. For comparison, Fig. 5 shows the fields at $T=15$ in the grating-free case. Both the forward signal and idler develop oscillatory features with no gain while the backward signal vanishes as there is now no coupling between the two signal fields.

In Fig. 6 we show the final fields at $T=15$ for a second simulation with $\Delta=8$, $\kappa=14$, and $\epsilon=-12$ [16]. Thus the system is now on the opposite side of the grating-free gain band. The behavior is similar in this case. At early times the weak fields become highly irregular and complicated, but eventually adopt simple peaked forms on the rear of the pump where they continue to grow uniformly. Note that the gain in this case is larger still than in Fig. 4 and that the signal fields $E_\pm$ are somewhat narrower than in the first case. We discuss the origins of these differences in Sec. VI. In both simulations, however, the location of the weak fields on the rear of the pump contrasts with growth in the nongrating case, for which the signal and idler always move to the center of the pump as discussed in Sec. III.

If the parameters are chosen such that the signal lies *inside* the gain band for the grating-free case, we observe even stronger amplification than in the cases just described and the signal again appears on the rear of the pump. The appearance of gain in this case is of course less striking than in the two out of gain band examples.

To see how the gain develops, we show the total energy in the signal and idler fields as a function of time for these two simulations in Fig. 7(a) ($\Delta=-16$, $\kappa=8$) and Fig. 7(b) ($\Delta=8$, $\kappa=14$). For both cases, we find an initial period where energy couples back and forth between the two signal fields but the total energy in the grating does not change significantly. The oscillations occur because the signal is initially chosen to have no energy in the backward mode. At later times, the oscillations die away and the energy increases almost exponentially with time. Comparing Fig. 7a with the corresponding time sequence of fields in Fig. 4 indicates that

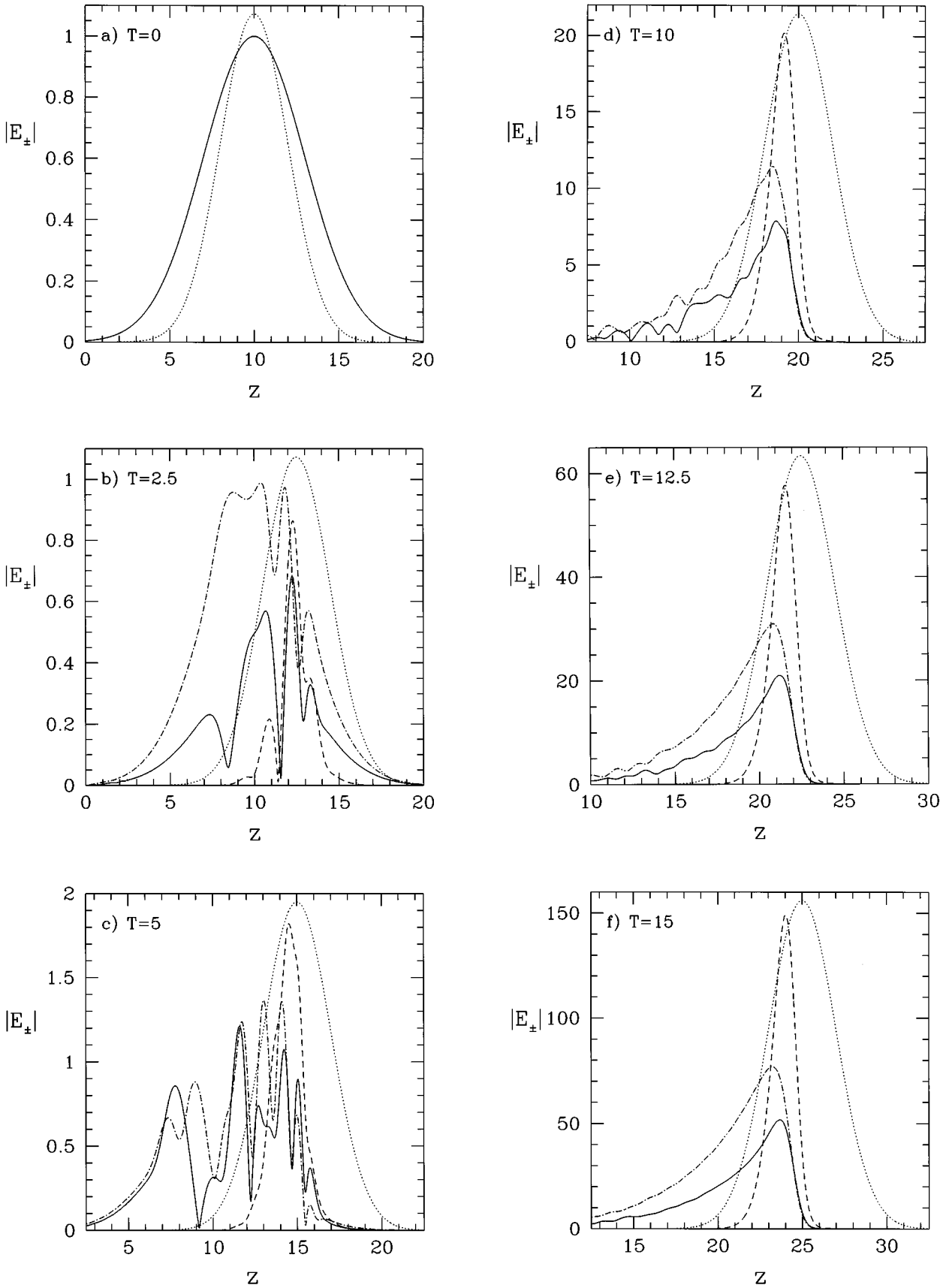

FIG. 4. (a)–(f) Time sequence of pulse evolution for $\Delta=-16$, $\kappa=8$. The fields are E_+ (solid), E_- (dash-dot), I (dash), P (dotted).

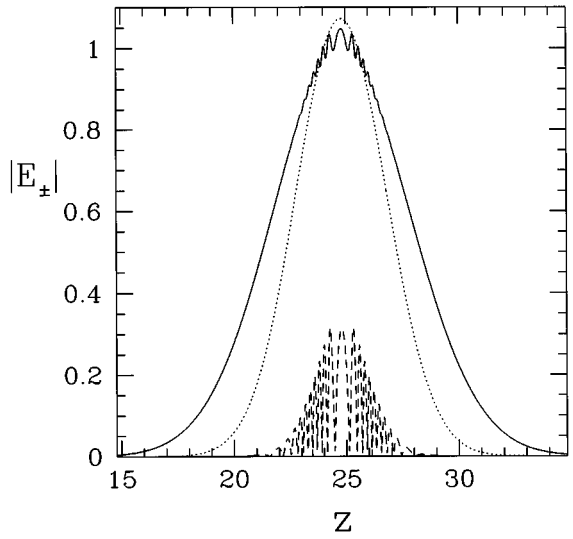

FIG. 5. Fields at $T=15$ for $\Delta=8$, $\kappa=0$. This plot should be compared with the equivalent time in the presence of the grating shown in Fig. 4(f).

the onset of growth occurs as the field structures begin to become simpler and concentrated at the rear of the pump. We have found this to be true in all simulations. Figure 7 also shows that the fields at $T=15$ are smaller in Fig. 4(f) than in Fig. 6 because the amplification both begins later and occurs more slowly in the first case than in the second.

The examples in Figs. 4 and 6 are typical of a very broad range of parameters. The initial pulse evolution can be highly involved but with sufficient time, the weak fields always experience growth and become located on the rear of the pump regardless of the relative sizes of Δ and κ. For all the simulations, however, the *rate* of growth and detail of the pulse *shapes* do depend on the parameters κ and Δ and for $\Delta \gg \kappa$ the initial period before amplification begins may be quite long. In this regime, the parametric amplification can be so poorly phase matched that it essentially plays no role

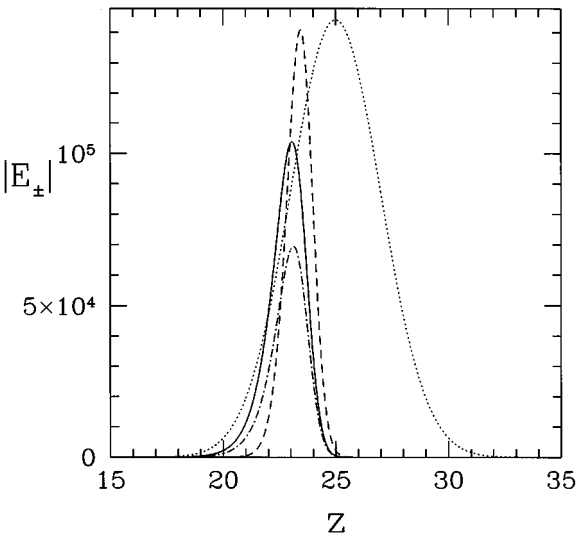

FIG. 6. Fields at $T=15$ for a simulation with $\Delta=8$, $\kappa=14$. The fields are E_+ (solid), E_- (dash-dot), I (dash), P (dotted).

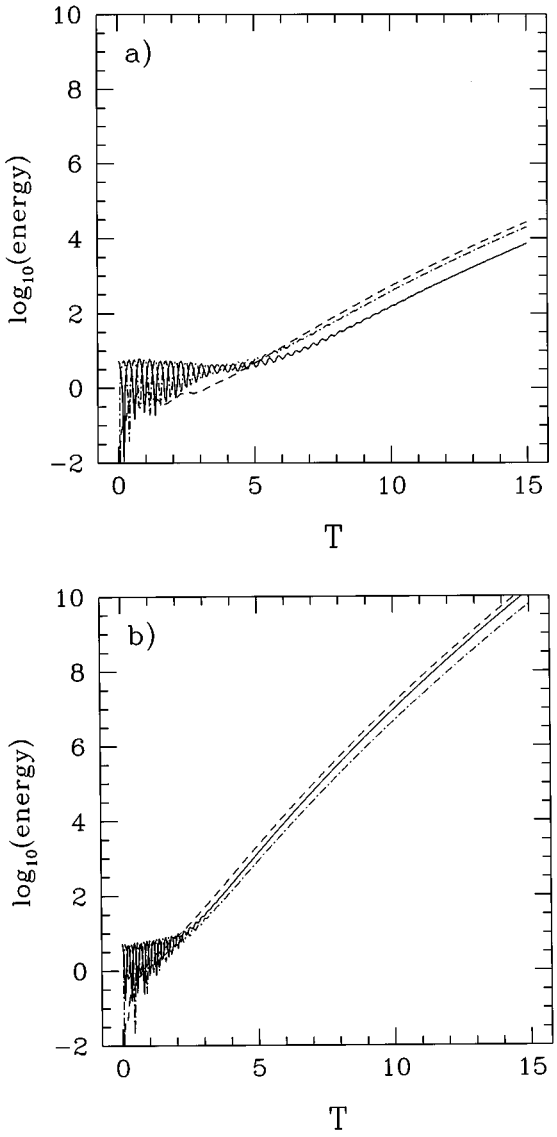

FIG. 7. Energy in fields as a function of time for (a) the simulation in Fig. 4 ($\Delta=-16$, $\kappa=8$) and (b) the simulation in Fig. 6 ($\Delta=8$, $\kappa=14$). Line styles are E_+ (solid), E_- (dash-dot) and I (dash).

and pulse-shaping effects such as the optical pushbroom described in Sec. I which rely only on XPM can operate [14,15]. Before considering the detailed dependence of the system on the mismatch and grating strength, we first describe the basic process that allows gain for such a broad range of parameters.

B. Mechanism for gain

The gain of course arises by a similar argument to that described for the cw case in Sec. II. There, the gain was enhanced for frequencies at which the grating introduced a wave vector shift compensating for the original mismatch Δ. In the pulsed case, we can expect self and cross-phase modulation to shift the frequencies of the different pulses over time so that similar effects may occur even if the initial frequencies are not phase matched by the grating. It is natural to suppose that the gain is largest if the signal spectrum moves to a point on the grating dispersion relation at which

the signal wave vector is shifted to the center of the gain band in the grating-free case. In other words, we might expect the signal to experience maximum gain if the grating induced wave vector shift produces an effective mismatch

$$\Delta_{\text{eff}} \equiv \Delta + \Delta k_s = -2\mu_{\max}, \tag{21}$$

or equivalently, if

$$\Delta k_s = \epsilon \tag{22}$$

[see Eqs. (19) and (20)]. In fact, as the weak fields become located on the rear of the pump [see Fig. 4(f)] rather than at the peak we should consider the strength of the pump at the peak of the signal. We thus introduce one further parameter: the pump-induced nonlinear detuning at the peak of the signal given by [see Eq. (4)]

$$\mu_s(T) = \Gamma f^2(z_s(T) - T), \tag{23}$$

where $z_s(T)$ is the position of the signal peak at time T. It is clear that $\mu_s(T) \leqslant \mu_{\max}$. Our final prediction then is that the gain should be maximized if $\Delta_{\text{eff}} \approx -2\mu_s$.

These arguments can be confirmed by examining the evolution of the frequencies of the different pulses. The signal detuning defined in Eq. (6) is determined numerically for each signal field by the expressions

$$\hat{\delta}_{\pm} = -\frac{\partial}{\partial T}\phi_{\pm}(z,T), \tag{24}$$

where the instantaneous phases $\phi_{\pm}(z,T)$ are defined by

$$E_{\pm}(z,T) = |E_{\pm}(z,T)| \exp[i\phi_{\pm}(z,T)]. \tag{25}$$

By analogy with Eqs. (24) and (25), we also define detunings for the idler $\hat{\delta}_i$ and pump $\hat{\delta}_p$ that represent deviations from the center frequencies ω_i and ω_p [see Eq. (11)]. It is also useful to consider the local wave numbers of the fields defined as

$$q_j = \frac{\partial}{\partial z}\phi_j(z,T), \tag{26}$$

where j runs over the symbols $+$, $-$, i and p for the signal, pump and idler fields, respectively.

Figure 8 shows the frequency detunings and wave vectors for all four fields as a function of time for the simulation of Fig. 4. All these parameters are measured at the peak of the forward signal field E_+. The detunings are shown corrected for the effects of SPM and XPM by the pump—the nonlinear index change induced by the pump shifts the band gap down in frequency (for a positive nonlinearity)—and are defined for $j = +, -, i, p$ by

$$\delta_j = \hat{\delta}_j + \sigma_j \mu_s(t), \tag{27}$$

where the caret denotes the directly measured detunings and $\sigma_j = 2$ for $j = +, -, i$ and $\sigma_p = 1$, indicating that XPM induces a shift twice as large as SPM [6] [see Eq. (6)].

We are now able to see how the frequency evolution supports our argument explaining gain. We stress again that the parameters are measured at the peak of the signal field

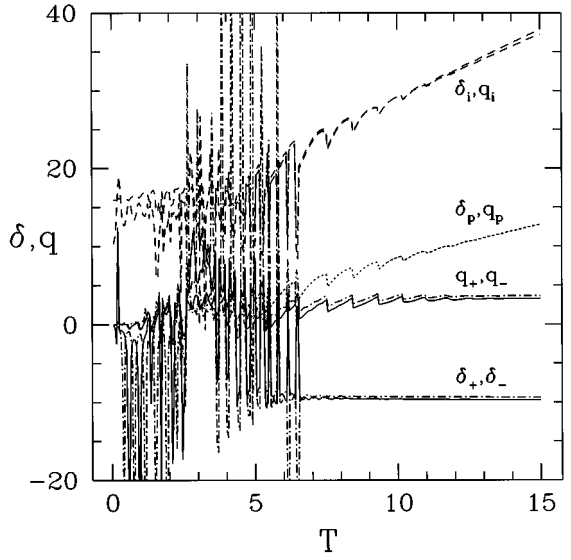

FIG. 8. Detuning and wave number of fields as a function of time for the time sequence in Fig. 4. Line styles indicate the same fields as in Fig. 4.

E_+. In Fig. 8, the pump detuning and wave number increase monotonically with time. This is because on the rear of the pump (where the signal peak is found), SPM induces a positive frequency shift. The detuning and wave number are exactly coincident ($\delta_p = q_p$) as the pump obeys the uniform medium dispersion relation $\omega_p = ck_p/\overline{n(\omega_p)}$. The idler shows similar behavior: in the initial period of complicated dynamics, δ_i and q_i have no simple relationship, but once strong amplification begins, these two parameters also become coincident since the idler obeys the uniform medium dispersion relation as well. The signal fields display very different behavior. In the initial period when energy oscillates between E_+ and E_-, the signal detunings also oscillate wildly. In this regime, the simple definition of detuning as the time derivative of the phase of each field is not well defined. However, at about $T = 6.5$, when the field oscillations die away and the gain begins, we find that both the detuning and wave vectors parameters become constant and remain so for the rest of the simulation. Moreover, from about the same time, we have $\delta_+ \approx \delta_-$ and $q_+ \approx q_-$ due to the strong coupling of the two signal fields by the grating. Note that q_+ and q_- represent changes in the absolute wave vectors of E_+ and E_-, rather than the absolute wave vectors themselves, so that although they refer to waves propagating in opposite directions, they may have the same sign. The behavior of the signal frequency and wave vectors strongly suggest that the onset of gain is related to the signal parameters nearing particular values. In contrast to the pump and idler, the signal detunings and wave vectors do not become coincident due to the dispersion of the grating. Noting in Fig. 8 that the signal detunings become fixed at a negative value and the wave vectors become fixed at a positive value, we see that the signal lies on the bottom right branch (d) of the dispersion relation in Fig. 2 and hence that the induced wave vector shift satisfies $0 < \kappa < \Delta k_s$. Recall from the first paragraph of Sec. V A that for this case, $\kappa = 8$ and the ''desired''

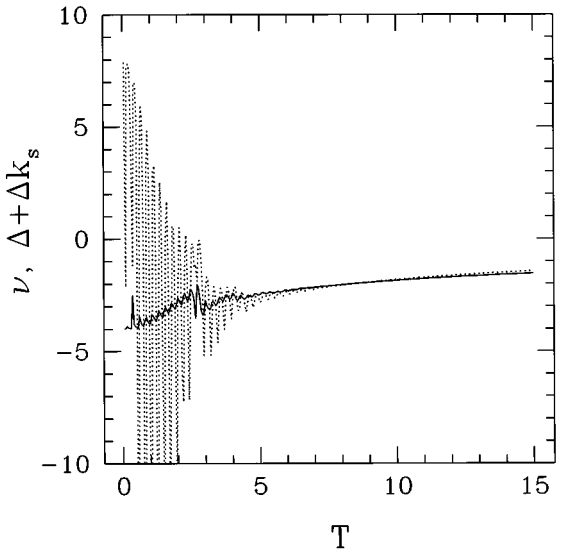

FIG. 9. Effective wave number mismatch $\Delta_{\text{eff}}=\Delta+\Delta k_s$ and $\nu=-2\Gamma|P(z_{\max})|^2$ as a function of time for simulation with $\Delta=8$, $\kappa=14$ (Fig. 6).

shift is $\epsilon=12>\kappa$. Thus the signal spectrum is in the correct quadrant of the dispersion relation to satisfy Eq. (22) and achieve phase matching.

This argument is quantitatively confirmed in Fig. 9 for the simulation corresponding to Fig. 6 where we take into account the location of the signal on the rear of the probe [see discussion following Eq. (22)]. The solid line shows the nonlinear detuning at the signal peak $\nu=-2\mu_s(t)$. We expect gain when the effective wave vector $\Delta_{\text{eff}}\approx-2\Gamma\mu_s(t)$. Now in the uniform medium with a constant phase velocity, we would have $\delta_+=q_+$, so with the grating included, $q_+-\delta_+$ represents the grating-induced wave vector shift Δk_s. Therefore we have $\Delta_{\text{eff}}=\Delta+(q_+-\delta_+)$. This quantity is shown with the dotted line. The convergence of the two lines at about the same time as gain is observed in Fig. 7(b) is a dramatic confirmation that the onset of gain is indeed associated with phase matching mediated by the grating.

We have stated above that the shift in detuning allowing growth is produced by XPM. On the rear edge of the pump however, XPM alone should generate positive frequency shifts whereas for the case in Fig. 1 the frequency shifts to negative values. In fact in the initial period of evolution before gain begins, the combined action of the nonlinear interactions and the grating leads to a very complicated frequency profile across the signal pulses. With sufficient time, frequencies allowing phase matching appear and are amplified. As growth occurs only at those frequencies, they quickly grow to dominate the spectrum.

The two simulations we have discussed demonstrate the signal spectrum moving to a point where gain is enhanced by grating-assisted phase matching. From many other examples, we have found this to be a very general behavior. Strong gain invariably occurs when the signal detuning and wave vector can compensate the initial mismatch ϵ. While the accuracy of this picture is not always as striking as for the case shown in Fig. 9, the variation in the frequency parameters with Δ and κ show trends that confirm its correctness. For example, consider the behavior as we vary κ if $\epsilon>0$: Our simple picture would predict that as κ increases, the value of $q_\pm$ for optimum phase matching would increase smoothly from negative values to positive values with $q_\pm=0$ when $\kappa=\epsilon$. Performing the simulations we typically find that while $q_\pm$ would not be zero exactly when $\kappa=\epsilon$, this is a reasonable approximation and the trend of $q_\pm$ increasing with κ is certainly obeyed. Given the complexity of the system, it is not surprising that we do not find perfect agreement with essentially cw arguments.

We have remarked above that for parameters placing the system *inside* the gain band, amplification also occurs. Further, if the signal is initially to one side of the gain band, the effects described above for the out of band cases now act to move the signal towards the center of the gain band where the amplification is largest.

VI. DEPENDENCE ON PARAMETERS

A. Rate of gain

Having established how the grating can facilitate amplification outside the grating-free gain band, we now turn to the detailed dependence of the pulse evolution on the system parameters κ and Δ. The most basic property is the rate at which gain occurs. In Fig. 10 we show the total energy in the signal field as a function of time for a range of different grating strengths and two wave vector mismatches—one far outside the grating-free gain band with $\Delta=8$ [Fig. 10(a)], and the other at the center of the gain band with $\Delta=-4$ [Fig. 10(b)]. For each mismatch, the total energy is plotted for 10 values of κ indicated by the labels on each figure and by the line styles described in the caption to Fig. 10. The basic appearance of the figures is as we would expect. For each value of κ, there is an initial period in which the signal energy is unchanged followed by a steady increase. We saw in Sec. V B that the initial period corresponds to the signal frequency and wave vector being shifted from the center of the photonic band gap to values at which the amplification is phase matched. Note that for some values of κ the initial period is negligible while for others it occupies the full time of the simulation. Moreover, the dependence of the initial period on κ is strikingly different for outside the gain band [Fig. 10(a)] compared to inside the gain band [Fig. 10(b)].

Discussing first the out of gain band case, Fig. 10(a) shows two obvious properties: both the rate of gain (given by the slope of the curves), and the time at which gain begins are functions of κ. Considering the rate of gain, we observe that during the period of steady growth, the slope increases monotonically with κ. This is simply interpreted in terms of the coupling of Bloch functions as described in Sec. II. Replacing Δk_s by ϵ in Eq. (10), we find the degree of overlap between the pump and the Bloch function occupied by the signal increases with κ and thus so does the rate of gain. Turning to the time at which the gain starts to act, we find a quite different dependence on κ. Amplification begins almost immediately for $\kappa=10$, 12, and 14, while there are initial periods without gain of varying length for $\kappa<10$ and $\kappa>14$. In fact we find both for this case of $\Delta=8$ and in general, that the initial time before gain begins increases with $|\kappa-|\epsilon||$. We can understand this from Eq. (8) which gives the detuning for perfect phase matching in terms of κ and the wave vector shift Δk_s. In the present case we have

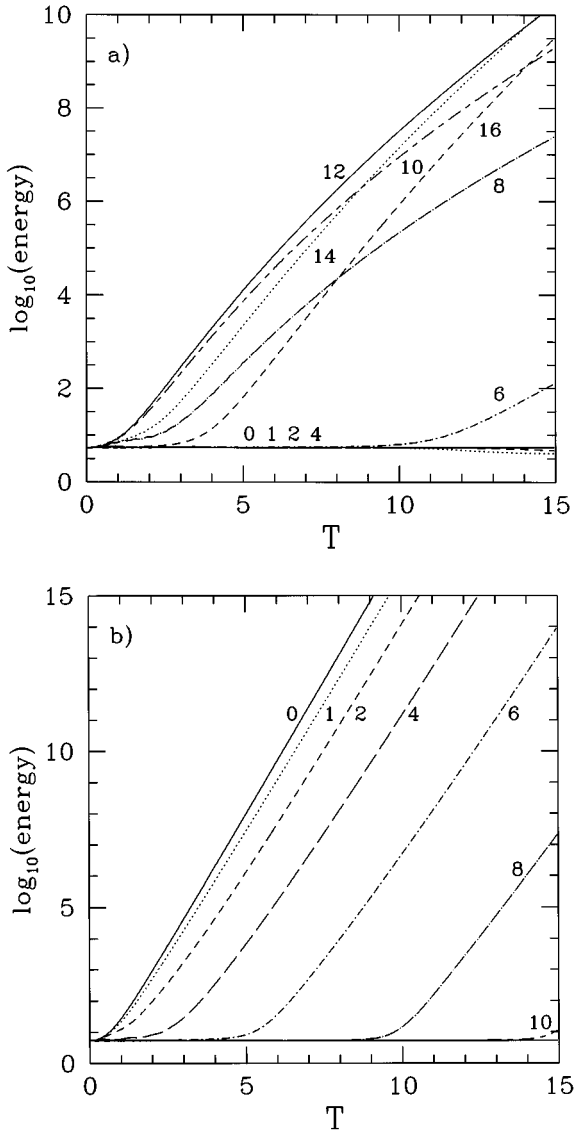

FIG. 10. Total signal energy as a function of time for varying κ. (a) $\Delta=8$, (b) $\Delta=-4$. The curves are labeled by κ which is also indicated by the line style as follows: $\kappa=0$ (solid), 1 (dot), 2 (short dash), 4 (long dash), 6 (dot-short dash), 8 (dot-long dash), 10 (short dash-long dash), 12 (solid), 14 (dot), 16 (short dash).

$\Delta k_s=\epsilon$. The wave vector shift needed for phase matching is of course $\Delta k_s=\epsilon$ [Eq. (22)]. Equation (8) shows that the detuning for phase matching occurs at the band edge [$\delta=-\,\mathrm{sgn}(\epsilon)\kappa$], if $\kappa=|\epsilon|$, and moves monotonically away from the band edge as $|\kappa-|\epsilon||$ increases (see Fig. 2). The time taken for the signal frequency to be shifted from the center of the band gap to the correct detuning for phase matching then must also increase with $|\kappa-|\epsilon||$, explaining the trend in the length of the initial period without gain. These trends in the rate of gain and time of onset are not peculiar to the parameters illustrated and are observed for all values of Δ outside the gain band.

Quite different behavior is observed for $\Delta=-4$ at the center of the gain band [Fig. 10(b)]. The rate of gain now *decreases* with increasing κ while the initial delay period increases monotonically with κ. The gain is fastest and begins immediately when the grating strength vanishes ($\kappa=0$). These effects are a consequence of the fact that the signal is already optimally phase matched in the absence of the grating. When κ is nonzero, the wave vector shifts induced by the grating *worsen* the phase matching, decreasing the gain rate. As the grating strength increases, the phase matching becomes ever worse so that the gain rate falls with increasing κ. In fact for $\kappa\neq 0$ with $\Delta=-4$, the pulse evolution is quite involved. As there is no frequency allowing perfect phase matching, there is no preferred frequency at which the signal should settle. Further the pulse shape does not become regular and single peaked in contrast to the results shown up till now. Far from the band gap, the small wave vector shift (to the branches marked a and c in Fig. 2) tends to zero, so the perturbation to the phase matching is less severe at large detunings. Near the center of the gain band therefore, amplification therefore tends to occur at large detunings. As κ increases, however, the band gap broadens and the signal detuning must be shifted by ever large amounts to reduce the magnitude of the grating induced wave vector shift. The time required to produce the detuning increases with its size, explaining the increase in the initial delay with κ. Indeed for $\kappa>12$, this time is longer than the simulation time $T=15$ [see Fig. 7(b)]. Note that this complex behavior occurs only for $\Delta\approx-4$. For other mismatches inside the gain band, the system operates similarly to the out of gain band case, and the dynamics are correspondingly simpler.

As is suggested by Figs. 10(a) and 10(b), the maximum gain observed in all our simulations is for the case of perfect phase matching in the absence of the grating ($\Delta=-4$, $\kappa=0$). This is simply because for all other cases, the grating is not directly connected to the parametric amplification process, but only acts to improve the phase matching—a grating cannot improve on perfect phase matching. The cw response of a finite grating differs from the present pulsed analysis in this respect—in the cw system there are many parameter values for which the output is larger with the grating than in a perfectly phase-matched medium of the same length [19]. This occurs because finite gratings can store large amounts of energy at Fabry-Pérot resonances [31]. Light tuned to such a resonance experiences a resonantly enhanced gain, larger than would occur with ideal phase matching in a uniform medium [19].

The Bloch functions occupied by the signal play another role in the gain process—determining the relative amplitudes of the two signal fields. Observe in Fig. 4(f) that the forward signal field is smaller than the backward field, while this situation is reversed in Fig. 6. This is simply a reflection of the relative contribution of forward and backward plane waves in the Bloch function as indicated by the vectors in Fig. 2 [see Eq. (9)]. In general, simulations show that as the ratio ϵ/κ varies, the relative size of E_+ and E_- varies in close correspondence to the content of the Bloch function at the point on the dispersion relation for optimum phase matching. Thus for $\epsilon/\kappa\ll 1$, E_+ is the dominant field in the signal, whereas for $\epsilon/\kappa\gg 1$, E_- dominates.

B. Pulse widths

The final characteristic of the pulse amplification we consider is the width of the signal and idler pulses. As pointed

out in Sec. III, if the signal lies in the gain band in the absence of the grating, the signal narrows indefinitely, becoming ever more tightly confined around the peak of the pump where the gain is largest. With the grating included, the signal narrows indefinitely if it lies inside the gain band. Outside the gain band, however, the pulse widths settle at constant values once the amplification begins.

The final width of the idler pulse shows relatively little variation amongst the simulations. The widths of the signal fields, however, vary significantly with the simulation parameters—compare the long tailed E_+ and E_- fields in Fig. 4(f) with the well-confined fields in Fig. 6. The variation in signal width shows two clear trends: it decreases with increasing κ and increases with increasing ϵ. Both these trends are closely linked to the group velocity of the signal as we now demonstrate. The pump can be thought of as ''depositing'' energy into the signal just to the rear of the pump peak. If the signal group velocity is close to the pump velocity, energy already in the signal does not significantly fall behind the pump, and the signal remains well confined. If the signal velocity is significantly less than that of the pump, energy already in the signal falls behind the pump producing an extended tail. Hence the signal pulse width should decrease with increasing group velocity. Note that in this argument the sign of the signal velocity is important—a negative large group velocity would cause the signal energy to quickly fall behind the pump and lead to a very broad pulse.

Now the group velocity of the pulse is given by the slope of the dispersion relation in Fig. 2, vanishing at the band edges and approaching the speed of light at large detunings. Once the gain is established, we expect the signal detuning to be approximately given by Eq. (8) with $k_s=\epsilon$. For this detuning, the group velocity is given by

$$v=\frac{\kappa^2-\epsilon^2}{\kappa^2+\epsilon^2}. \tag{28}$$

Note in particular, that for $\kappa<|\epsilon|$, the signal occupies one of the branches (b or d) and has a group velocity of opposite sign to the pump. Equation (28) shows that the signal velocity increases monotonically with κ, which by the argument of the previous paragraph shows that the signal width should decrease with increasing κ. Similarly, Eq. (28) shows that fixing κ, the group velocity should decrease, and thus the pulse width increase with increasing ϵ. We have observed both these trends in our simulations. The examples in Figs. 4(f) and 6 are consistent with this picture. For Fig. 4(f) the signal lies on the d branch (see Sec. V B), where the signal group velocity is negative and the width is large. In contrast, in Fig. 6 where the signal field lies on the a branch, the group velocity is positive and the pulse is narrow. These arguments also explain the fact that the fields grow on the trailing edge of the pump—unless perfectly phase matched in the absence of the grating, the signal group velocity must be smaller than the pump velocity and hence the signal lags the pump. The idler can only grow in company with the signal and thus is also found on the rear of the pump. Note the similarity of these arguments with the explanation for the relative rates of gain in Sec. VI A. In fact, as the rate of gain also increases with the overlap between the pump and signal Bloch function, we can expect strong gain to be associated with narrow signal pulses and vice versa—consistent with Figs. 4 and 6.

VII. DISCUSSION AND CONCLUSION

A. Self-locking gain

The principal result of this paper is the prediction of amplification of the signal at frequencies that lie outside the gain band in the absence of the grating. Of course, similar results are known for cw second harmonic generation and parametric amplification as discussed in Sec. II. There is, however, a striking difference between these problems and the present case of pulsed parametric amplification. In the cw problems, the gain is enhanced only if the input signal frequency is tuned to the point on the grating dispersion relation at which phase matching occurs. In the pulsed regime, this restriction does not apply—the input signal need only lie in the vicinity of the Bragg resonance. XPM generates new frequencies until part of the signal spectrum lies at the phase matched detuning and these frequencies are then amplified. Thus in the pulsed case, the gain may be said to ''self-tune'' or ''self-lock.'' While this is an appealing effect in its own right, it also has important consequences experimentally. Experiments in the cw regime would require precise tuning of the input signal (in fiber gratings typically to an accuracy of much less than one nanometer), especially if it is desired to hit a narrow Fabry-Pérot resonance. Pulsed experiments should be simpler in this regard, because the signal frequency may be chosen anywhere near the band gap. As the position of the Bragg resonance shifts with environmental factors such as temperature and strain, the self-locking could prove most useful.

In fact, the same effect could in theory occur without a grating—in a uniform medium, XPM can still shift the signal and idler around the *material* dispersion relation until phase matching occurs. The difference is one of scale. The grating dispersion is so strong that the error in phase matching can be accommodated by a shift in the signal detuning of the order of $v_g\kappa$, corresponding to a wavelength shift of perhaps less than a nanometer. In the absence of the grating, the signal wavelength would need to shift by many tens of nanometers to compensate for the same mismatch. This requires much longer propagation distances and makes for a much less striking effect.

B. Regime of the pushbroom

The self-locking idea leads to another important issue. From an experimental point of view, the geometry described in this paper is identical to that in our earlier work on the optical pushbroom [14,15,32]—a weak pulse and a strong pulse are launched into a grating and allowed to interact. In the pushbroom case, the frequency separation $\Delta\omega$ is assumed to be large, so that the wave vector mismatch Δ is also large and parametric amplification does not play a role. In this regime, the signal shows quite different behavior. Though it is not amplified, by the combined action of XPM and grating dispersion it is substantially compressed and swept out of the grating on the *leading* edge of the pump. In this paper, however, we have shown that the inclusion of the

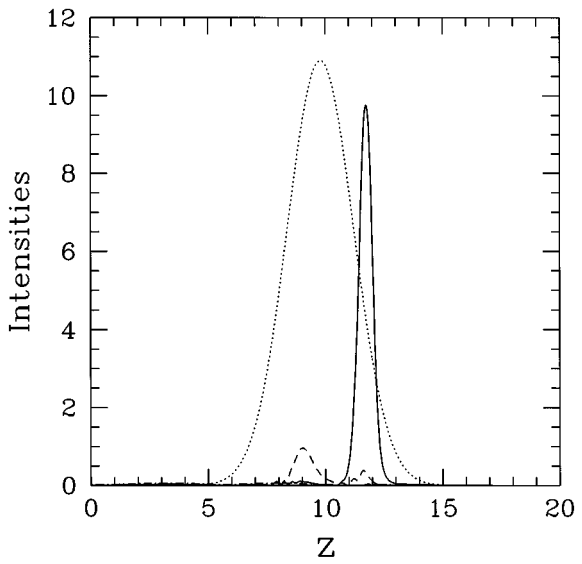

FIG. 11. Field intensities at $T=25$ for a simulation with $\kappa=1$, $\Delta=3.5$, $\mu_{\max}=2$. Line styles are $|E_+|^2$ (solid), $|E_-|^2$ (dash-dot), $|I|^2$ (dash), and $|P|^2$ (dotted). As usual, the pump is not shown to scale.

grating allows gain even when Δ is quite large. In what regime then, does the existing theory describing the push broom, which neglects parametric amplification, actually apply? Is it not true that regardless of the size of the mismatch parameter Δ, and therefore of the frequency separation $\Delta\omega$, we need only wait for the signal to be shifted to the phase-matched detuning before gain proceeds and swamps the compressive effects seen in the pushbroom?

The answer (which is happily negative), once more lies in the Bloch functions. For large $\Delta\omega$ implying (normally) large $\Delta \gg \kappa$, phase matching occurs on one of the distant branches (b or d) of the dispersion relation, and the longitudinal mode overlap between the pump and signal is so poor that the gain is negligible. Moreover, as Δ increases, it takes ever longer for the signal to be shifted to the phase-matched frequency in the first place, leaving aside the low gain when phase matching occurs. The final question is then exactly how large must Δ be before we can neglect the effects of parametric amplification. It is difficult to give a complete answer to this question, but the following criterion seems a reasonable estimate for order of magnitude purposes. Equation (10) gives the ''angle'' between the Bloch vectors representing the pump and signal. We suppose that the gain is negligible if the overlap is so small that $\cos\alpha \lesssim 0.1$. Then Eq. (10) immediately gives the condition that parametric amplification can be neglected if $|\epsilon/\kappa| \gtrsim 10$ [see Eq. (20)]. We show an example in Fig. 11. This figure shows the intensity of the fields at the end of a simulation with the same parameters used in Figs. 4 and 6 but with coupling strength $\kappa=1$ and $\Delta=3$. Thus $|\epsilon/\kappa|$ is only ≈ 4.7. However, the probe is substantially compressed and lies on the leading edge of the pump, as would be expected in the pushbroom regime [14,15]. The peak intensity of the idler is a factor 10 smaller than the peak signal intensity. Repeating the simulation without including parametric amplification produces a similar plot with no idler field. Thus for Δ yet larger, we should expect the idler field to be still smaller than in Fig. 11 and the existing pushbroom theory to be highly accurate. This is confirmed by other simulations. Finally, to give a sense of scale let us find the frequency separation that would be required to have $\Delta > 3$ for the experimental fiber parameters discussed in Sec. IV. There we chose the unit of length as the centimeter so that we seek $\Delta = 3\ \mathrm{cm}^{-1}$. With a pump wavelength of $\lambda_p = 1.064\ \mu\mathrm{m}$, from Fig. 3 we obtain a frequency separation of $\Delta\omega \approx 0.07\times 10^{15}\ \mathrm{s}^{-1}$ or a wavelength separation of about 30 nm.

C. Other issues

We have assumed throughout that the signal is tuned to the grating. For several reasons it might be preferable to have the idler close to the Bragg resonance instead. The action of the grating in phase matching would remain the same, but the role of the signal and idler fields would be reversed. For example, with our choice of the signal being close to resonance, the energy in the idler often exceeds that in the two signal fields, as can be seen in Fig. 7. Further, the idler is always narrower than the signal fields because its group velocity is not reduced by the presence of the grating (see Sec. VI B). Finally, whereas the signal would be partially reflected at the rear of the grating due to an impedance mismatch between the grating and the surrounding uniform medium, the idler would be completely coupled into the uniform medium. By making the idler resonant with the grating, these features would then become properties of the signal instead.

Throughout this paper, we have used an undepleted pump approximation. For some parameters, the gain can be so large that this approximation would begin to fail unless the initial signal amplitude was quite weak. An example is the simulation represented in Fig. 7(a), where the signal energy increases by nine orders of magnitude, and within the gain band the growth can be even more rapid. While it would be elementary to include pump depletion in our model, we have instead concentrated on the basic mechanism underlying the appearance of amplification outside the gain band.

A related issue is the problem of stimulated Raman scattering (SRS) of the pump in optical fibers. For powers of the order of 30 kW, SRS can be expected to be important over the typical length of fiber gratings [17]. SRS should introduce two main effects to the system. It clearly acts as a nonlinear loss to the pump. This effect would reduce the gain rate but is unlikely to qualitatively change the behavior. More significantly, the energy extracted from the pump by SRS appears as a Stokes wave over a broadband of longer wavelengths. For a pump wavelength of 1 μm, the peak of the Stokes wave spectrum is shifted by about 50 nm. This is comparable to the wavelength separations considered in this paper. Hence, SRS may deposit a significant fraction of the pump energy into the signal or idler, and should be included in a complete treatment. The present study, while neglecting SRS clearly elucidates the influence of the grating on parametric amplification and provides insight which would be much harder to extract from a model which included SRS from the beginning. In addition, SRS should be much less important in other geometries such as semiconductor gratings, for which the Raman gain band is usually much narrower than in glass. In that case, one could select a signal

frequency that was far from the generated Stokes wave.

The inclusion of a grating in a parametric amplification system profoundly changes the response of the system. Gain is permitted over a much wider range of parameters than in the corresponding uniform medium and produces large amplitude well-shaped pulses. The experimental design constraints needed to produce the effects described in this paper are quite demanding but as discussed in Sec. III, current optical fiber gratings with a high-powered Nd:YAG source should be sufficient to allow observation of grating-assisted amplification. The pulsed case has two clear advantages over experiments in the cw regime. First, there is the basic advantage that high pump powers are more easily produced in short pulses than for long periods. Moreover, in the cw regime, the system shows very fine spectral features due to narrow Fabry-Pérot resonances [19] which may complicate experiments. These narrow fringes are absent in the pulsed case which seems a promising system for experimentation.

ACKNOWLEDGMENTS

M.J.S. is grateful for financial support from the Australian Telecommunications and Electronics Research Board.

[1] F. Ouellette, Opt. Lett. **12**, 847 (1987).
[2] B. J. Eggleton, P. A. Krug, and L. Poladian, Opt. Lett. **19**, 877 (1994).
[3] R. Kashyap, S. V. Chernikov, P. F. McKee, and J. R. Taylor, Electron. Lett. **30**, 1078 (1994).
[4] P. A. Krug *et al.*, Electron. Lett. **31**, 1091 (1995).
[5] H. G. Winful, Appl. Phys. Lett. **46**, 527 (1985).
[6] C. M. de Sterke and J. E. Sipe, in *Progress in Optics XXXIII*, edited by E. Wolf (Elsevier, Amsterdam, 1994), Chap. III, pp. 203–260.
[7] C. J. Herbert and M. S. Malcuit, Opt. Lett. **18**, 1783 (1993).
[8] N. D. Sankey, D. F. Prelewitz, and T. G. Brown, Appl. Phys. Lett. **60**, 1427 (1992).
[9] A. Bieber, D. F. Prelewitz, T. G. Brown, and R. C. Tiberio, J. Opt. Soc. Am. B **13**, 34 (1996).
[10] B. J. Eggleton *et al.*, Phys. Rev. Lett. **76**, 1627 (1996).
[11] J. Lauzon, S. LaRochelle, and F. Ouellette, Opt. Commun. **92**, 233 (1992).
[12] S. Wabnitz, Opt. Commun. **114**, 170 (1995).
[13] S. LaRochelle, Y. Hibino, V. Mizrahi, and G. I. Stegeman, Electron. Lett. **26**, 1459 (1990).
[14] M. J. Steel and C. M. de Sterke, Phys. Rev. A **49**, 5048 (1994).
[15] M. J. Steel, D. G. A. Jackson, and C. M. de Sterke, Phys. Rev. A **50**, 3447 (1994).
[16] M. J. Steel and C. M. de Sterke, Opt. Lett. **21**, 420 (1996).
[17] G. P. Agrawal, *Nonlinear Fiber Optics* (Academic, San Diego, 1989).
[18] P. St. J. Russell and J.-L. Archambault, J. Phys. III (France) **4**, 2471 (1994).
[19] M. J. Steel and C. M. de Sterke, J. Opt. Soc. Am. B **12**, 2445 (1995).
[20] N. Bloembergen and A. J. Sievers, Appl. Phys. Lett. **17**, 483 (1970).
[21] C. L. Tang and P. P. Bey, IEEE J. Quantum Electron. **QE-9**, 9 (1973).
[22] A. Yariv and P. Yeh, J. Opt. Soc. Am. **67**, 438 (1977).
[23] V. A. Belyakov and N. V. Shipov, Phys. Lett. **86A**, 94 (1981).
[24] V. A. Belyakov, *Diffraction Optics of Complex-Structured Periodic Media* (Springer-Verlag, New York, 1992), Chap. 6, pp. 188–205.
[25] M. J. Steel and C. M. de Sterke, Appl. Opt. **35**, 3211 (1996).
[26] J. P. van der Ziel and M. Ilegems, Appl. Phys. Lett. **28**, 437 (1976).
[27] N. Broderick and C. M. de Sterke, Phys. Rev. E **51**, 4978 (1995).
[28] P. St. J. Russell, J. Mod. Opt. **38**, 1599 (1991).
[29] D. Marcuse, *Theory of Dielectric Optical Waveguides*, 2nd ed. (Academic, San Diego, 1991).
[30] C. M. de Sterke, K. R. Jackson, and B. D. Robert, J. Opt. Soc. Am. B **8**, 403 (1991).
[31] J. E. Sipe, L. Poladian, and C. M. de Sterke, J. Opt. Soc. Am. A **11**, 1307 (1994).
[32] C. M. de Sterke, Opt. Lett. **17**, 914 (1992).